Selective Stimulation of Sacral Nerve Roots for Bladder Control: A Study by Computer Modeling

Nico J. M. Rijkhoff, Jan Holsheimer, Evert L. Koldewijn, Johannes J. Struijk, Philip E. V. van Kerrebroeck, Frans M. J. Debruyne and Hessel Wijkstra

Abstract—**The aim of this study was to investigate theoretically the conditions for the activation of the detrusor muscle without activation of the urethral sphincter and afferent fibers, when stimulating the related sacral roots. Therefore, the sensitivity of excitation and blocking thresholds of nerve fibers within a sacral root to geometric and electrical parameters in tripolar stimulation using a cuff electrode, have been simulated by a computer model. A 3-D rotationally symmetrical model, representing the geometry and electrical conductivity of a nerve root surrounded by cerebrospinal fluid and a cuff was used, in combination with a model representing the electrical properties of a myelinated nerve fiber. The electric behavior of nerve fibers having different diameters and positions in a sacral root was analyzed and the optimal geometric and electrical parameters to be used for sacral root stimulation were determined. The model predicts that an asymmetrical tripolar cuff can generate unidirectional action potentials in small nerve fibers while blocking the large fibers bidirectionally. This result shows that selective activation of the detrusor may be possible without activation of the urethral sphincter and the afferent fibers.**

I. Introduction

FUNCTIONAL electrical stimulation can be used to restore bladder function in patients with serious neuropathic voiding disorders. There are several sites where stimulation can be applied to control the urinary bladder: the bladder wall (detrusor muscle) [3], [15], the pelvic nerves [16], sacral nerve roots [8] or the spinal cord [18]. Sacral root stimulation has been most successful in bladder evacuation and is commonly used in case of intact efferent innervation of the detrusor muscle. Sacral root stimulation can be performed by surface electrodes [38] or by implanted intradural [8], [19] or extradural [36] electrodes. The anatomy of the sacral roots allows their separation in ventral and dorsal branches. When implanted electrodes are used, stimulation can thus be restricted to the ventral roots (carrying most of the efferent fibers) and activation of dorsal root fibers (afferent pathways) can be avoided. However, a dorsal rhizotomy is usually performed in addition to reduce or abolish autonomic bladder reflex activity and to improve bladder responses [8], [36]. Attempts to empty the bladder by ventral sacral root stimulation have always been hampered by simultaneous contraction of the urethral sphincter. Unwanted movement of the lower limbs also occurs. This is due to the composition of the ventral sacral roots, which contain a mixed population of somatic fibers innervating some muscles of the lower limbs, the pelvic floor, the urethral and anal sphincter, and preganglionic parasympathetic efferents innervating the detrusor muscle. Since large fibers need a smaller stimulus for their excitation than small ones, activation of the small parasympathetic fibers (detrusor) is always accompanied by the activation of the larger somatic ones (urethral sphincter, lower limb muscles).

Several attempts have been made to overcome the problem of simultaneous sphincter activation. The poststimulus voiding technique described by Jonas and Tanagho [18] takes advantage of differences in biomechanical characteristics of smooth and striated muscle. The relaxation times (90% to 10% pressure reduction) of the striated sphincter muscle and the smooth detrusor muscle are 0.4 s and 13 s respectively. When stimulating with pulse trains (3–6 s ON, 6–9 s OFF), voiding is achieved between the pulse trains due to the sustained high intravesical pressure. This principle is used in a commercially available system developed by Brindley *et al.* [7], [8]. However, this artificial micturition pattern often causes voiding in spurts and supranormal bladder pressures, with the risk of damaging the upper urinary tract. A more drastic method is described by Schmidt *et al.* [30]. They have shown that the increased urethral resistance due to sacral root stimulation can be largely reduced by pudendal nerve section or block. This technique has been applied to patients [35], [36] with variable success. The major drawback of this technique is the need for irreversible surgery.

To avoid pudendal nerve section, Sweeney *et al.* [33], [34] introduced a technique to block reversibly the transmission of motor signals through the pudendal nerve to the urethral sphincter using the collision block principle. By stimulating the pudendal nerve with a special electrode, action potentials are generated which are propagated unidirectionally in a proximal direction. When those action potentials meet the distally propagating action potentials produced by simultaneous sacral root stimulation, the two signals collide and mutual annihilation occurs. In this way, the signals induced by sacral root stimulation cannot reach the sphincter muscle and the sphincter is thus prevented from contraction. A disadvantage is that distant stimulation sites are required. Furthermore, in both pudendal nerve section and blocking it is assumed that all efferent fibers innervating the human external urethral

Manuscript received February 9, 1993; revised January 25, 1994. This research was supported by the Dutch Kidney Foundation C 90.1032.

N. J. M. Rijkhoff, E. L. Koldewijn, P. E. V. van Kerrebroeck, F. M. J. Debruyne and H. Wijkstra are with the Department of Urology, University Hospital Nijmegen, The Netherlands.

J. Holsheimer and J. J. Struijk are with the Biomedical Engineering Division, Department of Electrical Engineering, University of Twente, The Netherlands.

IEEE Log Number 9401320.

0018–9294/94$04.00 © 1994 IEEE

sphincter are in the pudendal nerve, which is not generally agreed upon [23], [29].

Another technique takes advantage of the difference in excitation threshold between large fibers innervating the sphincter and small fibers innervating the detrusor muscle. Using a (high frequency) pulse train with an amplitude above the threshold for somatic fibers but below the threshold for parasympathetic fibers, the sphincter can be fatigued. This has been demonstrated in the baboon [7] and the dog [37]. After this fatiguing burst, a stronger stimulus must be given to activate the detrusor. A disadvantage of this method is that the sphincter is not relaxed to the prestimulus tone during detrusor activation, due to the presence of fatigue resistant slow-twitch muscle fibers [37].

Cocontraction of skeletal muscles in the lower limbs is not reduced by these methods. Moreover, sacral root stimulation can be applied only in patients with a complete spinal cord transection, or in patients with an incomplete lesion but without pelvic pain sensation. Other patients feel pain during stimulation which is probably due to the stimulation of afferent fibers present in the ventral roots [11], [27].

The above-mentioned problems could be solved if the induced undesired activity in the concerned fiber groups could be arrested. This is possible with the anodal block technique [1], [6], [12], [17]. Near an anode the membranes of nerve fibers are hyperpolarized by the anodal current. If the nerve membrane is sufficiently hyperpolarized, action potentials cannot pass the hyperpolarized zone and are annihilated. As anodal current is increased, the larger fibers will be blocked before smaller ones; thus anodal blocking can be used to obtain a selective fiber blockade.

This method would avoid activation of the urethral closure mechanism without the need for extra surgery or additional electrodes. Moreover, it may result in a more physiological evacuation of urine, including lower peak pressures than are obtained during poststimulus voiding. It may also eliminate cocontraction of skeletal muscles in the lower limbs during stimulation. By blocking most sensory fibers proximal to the cathode, pain sensation in patients with preserved pelvic pain sensitivity may be reduced. Thereby, the technique of sacral root stimulation could be applied to more patients suffering from neuropathic voiding disorders. The application of anodal block in sacral root stimulation has been described by Brindley *et al.* [6], [7], who used asymmetrical tripolar electrodes. Results have not been reported apart from the conclusion "we have not yet succeeded in making the method well enough in patients for every day use."

Tripolar cuff electrodes consisting of circular contacts embedded on the inner surface of a cylindrical insulating tube (Fig. 1(a)) can be used to achieve both excitation and anodal block. They can be wrapped around a nerve bundle and have been shown to be successful in various blocking experiments [12], [17], [32]. The design of a cuff electrode as a neural prosthesis, however, still mainly relies on rules-of-thumb and improvements by animal or clinical testing.

Few attempts have been made to analyze the behavior of nerve fibers in a cuff electrode and the influence of geometric and electrical parameters by modeling. Altman and Plonsey [2] presented a simple model, but without a systematic evaluation of main parameters (e.g., electrode separation, cuff inner diameter). They assumed a uniform axial current density inside the cuff, as well as an isotropic and homogeneous medium. A more detailed approach of the volume conductor has been made by Ferguson *et al.* in an initial study [13].

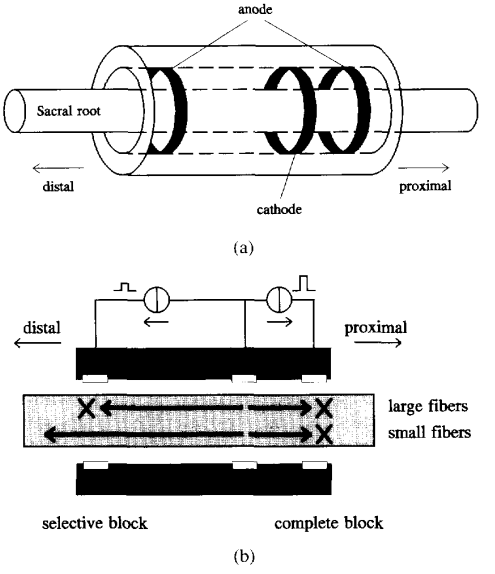

Fig. 1. (a) Asymmetrical tripolar cuff electrode. (b) Functional goals of the cuff. Complete block at proximal anode, selective block at distal anode.

We developed a model to calculate both the electric potential field generated by a tripolar cuff electrode with circular contacts and the responses of myelinated nerve fibers to this field. The effects of various geometric and electrical parameters on the behavior of the nerve fibers was simulated. In this way the parameters necessary to achieve maximum selectivity, minimum dimensions and minimum current were determined. The results of the modeling study on sacral root stimulation are presented in this paper.

II. Methods

A. Introduction

The cuff electrode will be placed intradurally around a sacral ventral root. The cuff should elicit solely bladder contraction; activation of the urethral sphincter should be avoided. In order to suppress reflex spasms and pain sensation, stimulation of afferents in the ventral root [27] and antidromic stimulation of the parasympathetic fibers [22] should also be avoided. These effects can be accomplished by combining: **A)** excitation of all myelinated fibers near the cathode, **B)** abolition of induced action potentials in the somatic fibers, without affecting the parasympathetic fibers, by hyperpolarization near the anode placed distally to the cathode, and **C)** abolition of induced action potentials in all myelinated fibers by hyperpolarization near the anode placed proximally to the cathode (Fig. 1(b)). The range of fiber diameters to be excited and blocked

proximally should thus include the parasympathetic fibers and the somatic fibers.

While only the large fibers must be blocked at the distal anode, at the proximal anode all fibers must be blocked. Since the stimulus amplitude needed for blocking will increase as the fiber diameter decreases [12], the proximal anode should inject more current into the medium than the distal one. When equally-spaced contacts (symmetrical configuration) are used, unequal anodal currents will lead to different electric potentials at the two outer contacts (anodes) and flow of electrical current not only inside, but also outside the cuff. An external current leak can have two disadvantageous effects. First, a virtual cathode [17] will be formed at the end of the cuff where the current leaves the nerve root. If the current is sufficiently high, the virtual cathode will excite (large) fibers and thus undo the blockage. Secondly, other nerve roots in the vicinity of the cuff can be stimulated. In order to confine the stimulus current to the inside of the cuff, an asymmetrical tripole with two synchronized current sources should be used. If the conductivity inside the cuff and the cuff inner diameter are uniform along the length of the cuff, the anodal current ratio should be the reciprocal of the intercontact separation ratio in order to obtain the same potentials at the two anodes and no leakage of current outside the cuff.

The calculation of the effects of electrical stimulation on myelinated fibers in a sacral root consisted of two steps. In the first step, the potential field generated by a cuff electrode was determined using a volume conduction model which incorporated inhomogeneities and anisotropy. In the next step, the response of a myelinated nerve fiber model, at a specific position in the nerve bundle, to the stimulus induced potential field was calculated.

B. Volume Conduction Model

The electric potential field can be calculated by solving Poisson's equation with appropriate boundary conditions. The volume conductor is rotationally symmetrical, the axis of the cuff electrode and nerve being the axis of symmetry of the model. Therefore, Poisson's equation can be expressed in cylindrical coordinates and the 3-D field problem is reduced to a 2-D problem (see Appendix). At the axis of symmetry ($r = 0$) the Neumann boundary condition has been applied, while the other 3 boundaries have been considered as Dirichlet boundaries.

In our volume conduction model a cylindrical nerve root with a diameter of 1.4 mm [26] is assumed (compartment 1 in Fig. 2). Compartment 2 represents the insulating part of the cuff electrode, which has a thickness of 0.6 mm. Compartment 3 represents the metal contacts (thickness: 0.2 mm). Medium 4, surrounding cuff and nerve, represents the cerebrospinal fluid (CSF, intradural space). Compartment 5 at the border of the model is a compressed representation of the tissues at a large distance from the nerve (thickness: 1 mm).

Compartments 2–5 are isotropic while compartment 1 (nerve root) is anisotropic with conductivity σ_z in a direction parallel to the bundle axis and σ_r perpendicular to this axis. The conductivities of nerve and CSF were obtained from

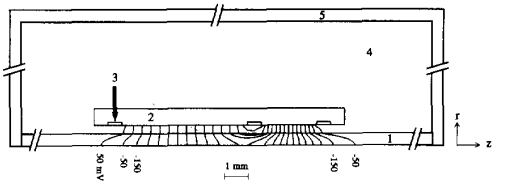

Fig. 2. The 2-D volume conductor model. 1: nerve, 2: cuff, 3: metal contact, 4: cerebrospinal fluid, 5: boundary layer. Isopotential lines plotted in the volume conductor model. Contact separation: 3 mm and 6 mm, inner diameter: 2.4 mm, I_{cat}: 5.4 mA, $I_{prox\ an}$: 3.6 mA, $I_{dist\ an}$: 1.8 mA. Isopotential range: 50–1450 mV.

TABLE I
CONDUCTIVITIES OF THE MEDIA IN THE COMPARTMENTS OF THE VOLUME CONDUCTOR MODEL

Model compartment	Tissue	Conductivity [S/m] σ_r	σ_z
1	nerve	0.083	0.6
2	cuff	0.0017	0.0017
3	contact	6	6
4	csf	1.7	1.7
5	boundary	0.01	0.01

Geddes and Baker [14]. With respect to these values, the conductivities of cuff and contacts have been given a low and a high value, respectively. All conductivities are summarized in Table I.

The current sources have been modeled as infinitely small circles. When modeling an electrode contact with finite width, the applied current is distributed evenly over all grid points of that contact in the 2-D model. The high conductivity of the contacts allows for a nonuniform current density over the boundary between the contact and CSF. A circular contact consisting of one grid point is called a contact with zero width.

An example of the potential distribution is shown in Fig. 2. At the lower boundary of the model (the axis) the isopotential lines are normal to this boundary, which means that no current crosses the symmetry axis of the model (Neumann boundary condition). The spacing of successive isopotential lines between the cathode and proximal anode is nearly constant. The spacing of isopotential lines between the cathode and the distal anode is also nearly constant but larger, indicating a lower current density between these contacts. A small amount of current will leak away to the three Dirichlet boundaries ($V = 0$) because the impedance between anode and boundary is not infinitely high. Therefore the potential at the anodal contacts is a little above zero. This explains the $+50$ mV isopotential line at the extreme left. The potential difference between the two anodes was 6.4 mV.

C. Nerve Fiber Model

The nerve fiber model was adopted from McNeal [20]. He used the Frankenhaeuser-Huxley equations, derived from myelinated frog nerve, to describe the dynamic electric behavior of the membrane at the nodes of Ranvier. The properties of mammalian nerve fibers however, are different. Most notable is that voltage dependent potassium channels, shown in amphibians, are absent at the nodes of Ranvier in the mammal, and

TABLE II
PARAMETERS FOR MYELINATED NERVE MODEL

ρ_a	0.7 Ωm	intra axonal restivity
c_m	0.02 Fm^{-2}	nodal membrane capacitance
l	1.5 μm	nodal length
L/D	100	ratio of internodal distance to outer fiber diameter
d/D	0.7	ratio of axon to outer fiber diameter

that the membrane leak conductance is larger [9], [10]. Therefore, we adapted the equations of membrane kinetics according to Chiu *et al.* [10]. All temperature-dependent parameters were scaled to 37°C (for equations and parameters, see [31]). The ratio of the internodal length and the fiber diameter (L/D) was set at 100, according to Schalow [27]. Other fiber parameters are summarized in Table II. The responses of two fibers have been calculated with this model: one with a diameter of 4 μm, representing the parasympathetic fibers, and a 12 μm fiber representing the somatic fibers. The small axon was modeled with 51 excitable nodes and the large axon had 17 excitable nodes. In practice both the detrusor and the urethral sphincter are innervated by a small range of fiber diameters. Schalow [27], [28] showed a clear distinction between the two diameter ranges (detrusor: 2–5 μm, sphincter: 9–13 μm).

Because small and large fibers are distributed throughout the whole nerve root, thresholds will vary as a function of the position inside the bundle. Therefore, threshold values of each fiber type were calculated at two extreme fiber positions: the axis and the edge of the nerve bundle.

Rectangular monophasic current stimuli have been used for the excitation and blocking of the nerve fiber models, although it has been shown that blocking by this pulse shape may be ineffective, due to the phenomenon of anodal break excitation (see Section IV).

In order to determine how the electrode dimensions and stimulus current can be minimized, the effect of contact separation and cuff inner diameter on the thresholds for blocking and excitation have been simulated using a symmetrical cuff electrode. Using electrodes with the optimal dimensions, we simulated the influence of pulse duration and asymmetrical configurations to achieve maximum selectivity.

III. RESULTS

Fig. 3 shows the response of a 4 μm fiber at the axis of the nerve bundle to the field shown in Fig. 2. Depolarization is shown with a bar above the line while hyperpolarization is indicated below the line.

With increasing time there is successive depolarization of nodes at the distal, but not the proximal side, indicating a unidirectional propagating action potential. The hyperpolarization at the proximal anode is strong enough to arrest propagation (anodal block).

A. Relation Between Contact Spacing and Excitation/Blocking Threshold

The reaction of a myelinated nerve fiber to extracellular stimulation is related to the second order difference quotient of the extracellular potential ϕ outside each node. This quotient

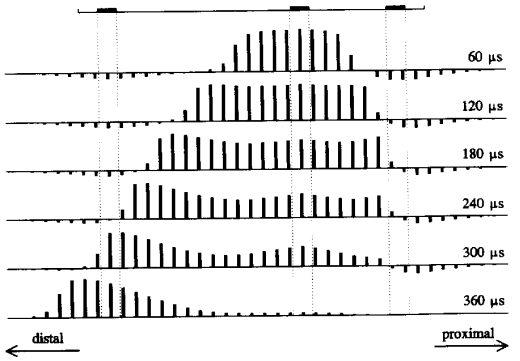

Fig. 3. Response of a 4 μm fiber to the field shown in Fig 3. It shows the deviation of the membrane potential from the resting potential at each node of Ranvier after initiation of a rectangular pulse of 320 μs. The nodal potentials are shown at 6 intervals of 60 μs after initiation of the pulse. At the top the cuff and the position of the contacts relative to the nodes of Ranvier are shown.

$\Delta^2\phi/\Delta z^2$ is called activating function by Rattay [24], [25]. Although fiber parameters also influence the amount of current needed for excitation, the activating function can be used to qualitatively study the influence of the geometry of multipolar electrodes. In a symmetrical tripolar configuration with identical anodal currents, the following qualitative relation between contact spacing and excitation threshold should theoretically be obtained. At large contact separations both the cathode and the two anodes can be considered as monopoles and the excitation threshold is fully determined by the cathodal field (Fig. 4(a)). When contact separation is decreased, the positive sidelobes of the anodes overlap with the positive central peak of the activating function of the cathode (Fig. 4(b)), which increases this peak value and decreases the excitation threshold. When contact separation is decreased further, the negative central peaks of the anodal activating functions overlap with the positive central peak of the cathodal activating function, which increases the excitation threshold (Fig. 4(c)). The qualitative relation between contact spacing and blocking threshold is identical to the relation between contact spacing and excitation threshold and can also be derived by the overlap of anodal and cathodal activating functions.

In a symmetrical cuff configuration we calculated the influence of contact separation on the excitation and blocking thresholds of 4 μm and 12 μm fibers positioned at two extreme positions: at the axis of the nerve bundle and at its boundary. The cuff inner diameter was 2.0 mm. The circular contacts had zero width. When the excitation threshold was calculated, the fibers always had a node of Ranvier in the plane of the cathode. A pulse width of 200 μs was used. When the blocking threshold was calculated, a node of Ranvier was in the plane of the blocking anode. Because a symmetrical configuration was used, the behavior at the two anodes will be the same. The pulse width for blocking was 600 μs, which was long enough to achieve a minimum blocking threshold.

The results in Fig. 5(a) show that the fibers at the axis of the bundle (curves b and d) exhibit the expected relationship. The fibers at the border of the bundle (a, c) are close to the contacts and the overlap of activating functions will therefore

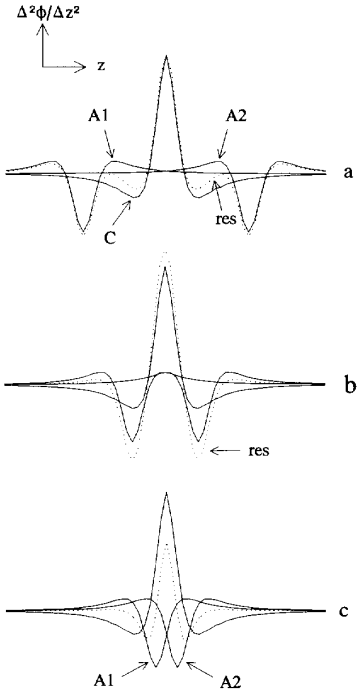

Fig. 4. Activating functions (AF's) of two anodes (A1 and A2) and a cathode (C) and the resulting AF (res) at three different contact separations. (a) Contact separation is relatively large and individual AF's can be considered as monopoles. The individual positive and negative peaks are as high as the resulting AF. (b) Contact separation decreased. Peaks of the resulting AF are increased by the sidelobes of individual anodal and cathodal AF's. (c) Contact separation further decreased. Anodal and cathodal peaks overlap and decrease the peaks in the resulting AF.

appear at smaller contact separations than shown in Fig. 5(a). It is shown that the threshold of a fiber of a given diameter at the axis of the bundle is higher than at the border. When the contact separation is increased from 1.8 mm to 6.0 mm the ratio between threshold at axis and threshold at border for a 12 μm fiber decreases from 2.7 to 1.6 and for a 4 μm fiber from 4.3 to 2.9. Fig. 5(a) also shows that when a contact separation larger than 2.1 mm is used, activation of all 12 μm fibers without activation of any 4 μm fiber is possible.

Fig. 5(b) shows the relation between contact spacing and blocking threshold. The threshold of a fiber with a given diameter is higher at the axis of the bundle than at its border. For a 12 μm fiber the ratio of threshold at axis to threshold at border decreases from 3.8 to 1.8 and for a 4 μm fiber from 5.9 to 3.3 when the electrode separation increases from 1.8 to 6.0 mm. Fig. 5(b) also indicates the possibility of blocking all 12 μm fibers without blocking any 4 μm fiber when the contact separation is 2.1 mm or greater.

To get an impression of the range of contact separations and stimulus currents which form an "operating window" for selective activation of small fibers with a tripolar cuff electrode, excitation and blocking threshold were plotted versus contact separation in Fig. 5(c). The electrode had an asymmetry ratio of 2. All thresholds are shown as a function of cathodal current. If the asymmetry ratio equals 2, the cathodal current is three times the current at the distal anode. Thus, to present the blocking thresholds as a function of the cathodal current in Fig. 5(c), all blocking thresholds of Fig. 5(b) have been multiplied by 3.

The operating window of this configuration is bordered by three lines. On the left, the window is bordered by solid line d (excitation threshold of 4 μm fiber at axis of nerve) and broken line b (block threshold of 12 μm fiber at axis), and on the right by broken line c (block threshold of 4 μm fibers at border of nerve bundle). The width of the window decreases from 0.82 mA (from 0.88 to 1.7 mA) at 6 mm separation to 0 mA at 2.2 mm contact separation. Decreasing the asymmetry ratio will decrease the window because the broken lines (threshold block) will move to the left, but the solid lines (threshold excitation) will not. With ratio = 1 (symmetrical) the width of the window is decreased to 0.26 mA (from 0.88 to 1.14 mA) at 6 mm contact separation. Increasing the ratio above 2 will widen the window between broken lines b and c. However, the whole window moves to the right, so the electrode operates at a higher cathodal current. As shown in Fig. 5(c), the minimum cathodal current is determined by broken line b and solid line d. The largest window under the condition of minimum cathodal current is obtained if the ratio equals 2.

One of the aims of the cuff electrode is to block all action potentials initiated at the cathode at the anode proximal to the cathode. In order to determine the minimum contact separation resulting in a complete block, it is sufficient to consider the fiber with the highest blocking threshold. Under the conditions of this study, this is a 4 μm fiber at the axis of the nerve bundle. Fig. 5(d) shows the relation between contact separation and blocking threshold for a 4 μm fiber for three cuff diameters. When cuff diameter is decreased from 2.8 mm to 2.0 mm, the contact separation at which the minimum blocking threshold occurs decreases from 5.5 mm to 4 mm; however the minimum is not very pronounced. Threshold increases steeply below 3 mm contact separation. From these results we may conclude that the minimum contact separation for blocking all fibers at a low stimulus current is approximately 3–4 mm. We chose a separation of 3 mm because this makes the electrode smaller while the currents only increase 4.7%, 5.1% and 6.3% for 2.0 mm, 2.4 mm and 2.8 mm cuff inner diameter respectively.

B. Relation Between Cuff Inner Diameter and Excitation/Blocking Threshold

The influence of the cuff inner diameter on excitation and blocking threshold was calculated for a 6 mm contact separation and contact width of zero. The results in Fig. 6(a) show that excitation thresholds increase when the cuff inner diameter increases. The relative difference in threshold for a fiber at the axis and a fiber at the border of the bundle decreases with increasing cuff inner diameter. If the diameter increases from 2.0 mm to 3.6 mm, this relative difference decreases from 1.6 to 1.4 for a 12 μm fiber and from 2.9 to 1.8 for a 4 μm fiber. Moreover, the selectivity (stimulation of all 12 μm fibers and no 4 μm fibers) increases with increasing cuff diameter. If the cuff diameter increases from 2.0 mm to 3.6

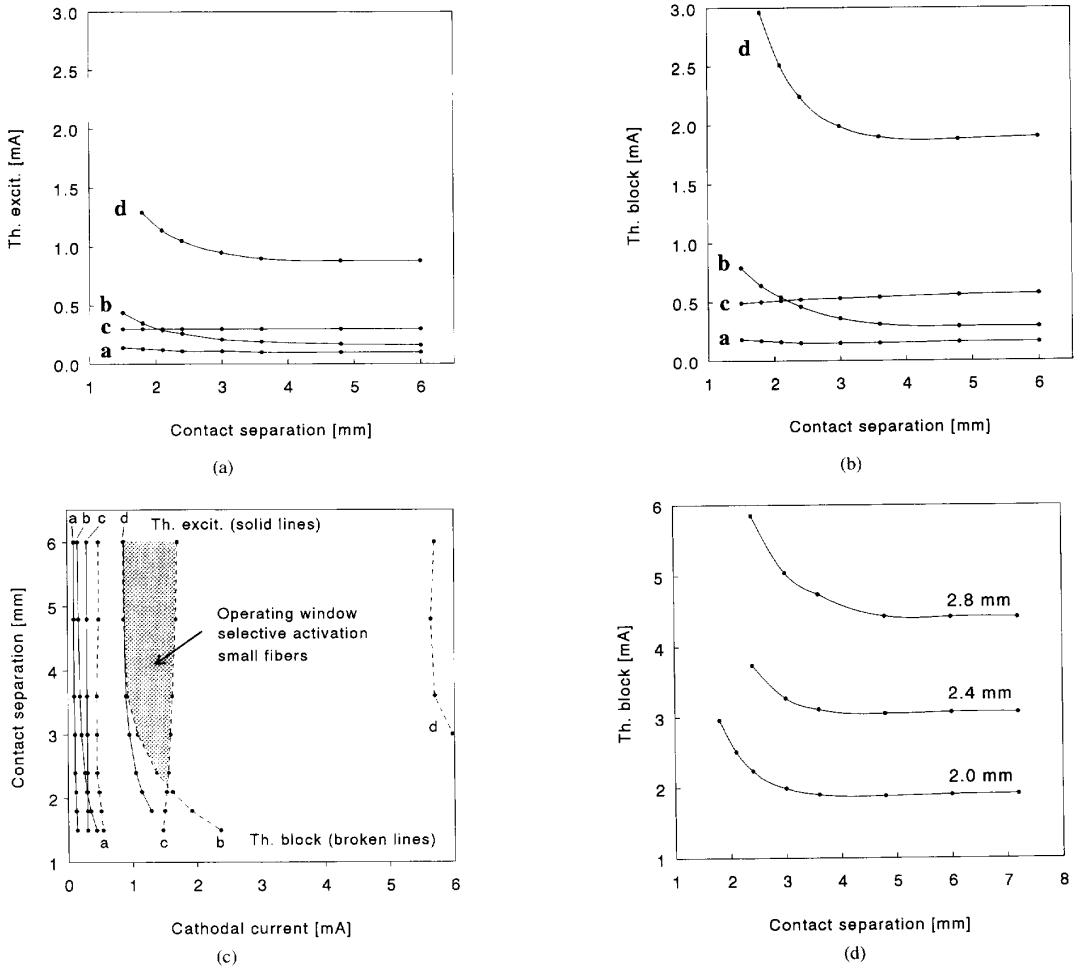

Fig. 5. (a) Excitation threshold (cathodal current) as a function of contact separation. Zero contact width, cuff inner diameter: 2 mm, sacral root diameter: 1.4 mm. a: 12 μm fiber at border of nerve bundle, b: 12 μm fiber at axis of nerve bundle, c: 4 μm fiber at border of nerve bundle, d: 4 μm fiber at axis of nerve bundle. (b) Blocking threshold (anodal current) as a function of contact separation. Cuff inner diameter: 2 mm, zero contact width. a–d: Fiber positions, see (a). (c) Excitation and blocking thresholds of small and large fibers at several contact separations as function of cathodal current for an asymmetrical tripolar cuff electrode. Hatched area is operating window for selective activation of small fibers. Asymmetry ratio: 2, cuff inner diameter: 2 mm, zero contact width. a–d: Fiber positions, see (a). (d) Blocking threshold (anodal current) as a function of contact separation for a 4 μm fiber positioned at the axis. Cuff inner diameters: 2.0, 2.4 and 2.8 mm.

mm, the ratio (threshold 4 μm fiber at nerve border/threshold 12 μm fiber at nerve axis) increases from 1.9 to 3.1.

Fig. 6(b) shows that blocking thresholds also increase with increasing cuff inner diameter. Over the whole range of diameters it is possible to block all 12 μm fibers without blocking any 4 μm fiber. The selectivity ratio (threshold 4 μm fiber at nerve border/threshold 12 μm fiber at nerve axis) increases from 2.0 to 3.7 if the inner diameter increases from 2.0 mm to 3.6 mm.

In Fig. 6(c) the data of Fig. 6(a) and (b) is combined in the same way as in Fig. 5(c) for a configuration with an asymmetry ratio of 2. It shows an "operating window" for selective activation of small fibers between solid line d (excitation threshold of 4 μm fiber at axis of nerve) and broken line c (block threshold of 12 μm fiber at border). The width of the window increases from 0.82 mA (0.88–1.7) to 9.9 mA (4.0–13.9) if the cuff inner diameter is increased from 2.0 mm to 3.6 mm, at the cost of an increasing cathodal current. An asymmetry ratio above 2 will increase the width of the window but will also increase the cathodal current.

C. Effect of Pulse Duration on Blocking Threshold

The ratio of conduction velocities of a 4 μm fiber and a 12 μm fiber is about the same as their diameter ratio [4]. Therefore, it takes about twice as long for an action potential of a 4 μm fiber to propagate from cathode to anode as it takes for an action potential of a 12 μm fiber. Thus, it may be possible to block a 12 μm fiber and not a 4 μm fiber, solely by selecting the right pulse duration. To assess this duration we modeled two asymmetrical cuff configurations (cuff inner diameter: 2.4 mm), one having a ratio of 2 between contact separations (3 mm and 6 mm) and one with a ratio of 3 (3 mm

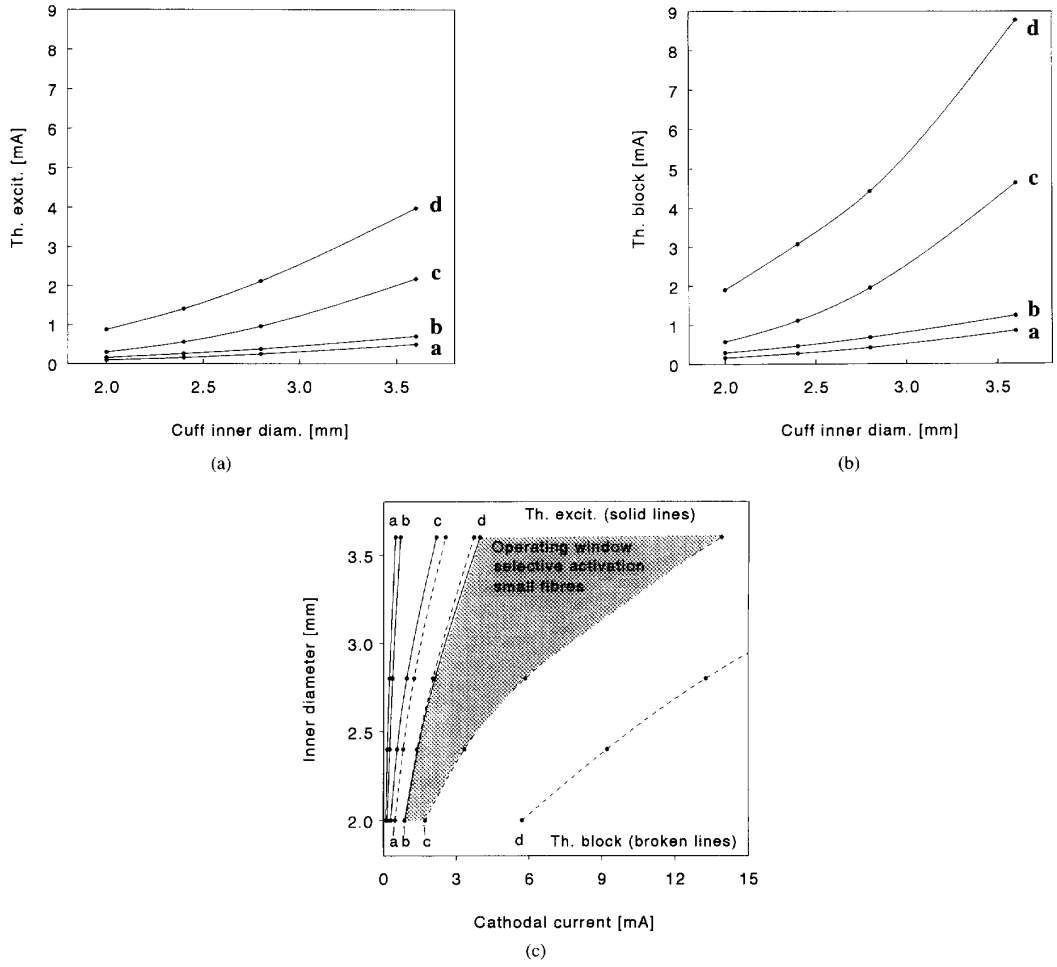

Fig. 6. (a) Excitation threshold (cathodal current) as a function of cuff inner diameter. Contact separation: 6 mm, zero contact width. a–d: Fiber positions, see Fig. 5(a). (b) Blocking threshold (anodal current) as a function of cuff inner diameter. Contact separation: 6 mm. a–d: Fiber positions, see Fig. 5(a). (c) Excitation and blocking thresholds of small and large fibers at several cuff inner diameters as a function of cathodal current for an asymmetrical tripolar cuff electrode. Hatched area is operating window for selective activation of small fibers. Asymmetry ratio: 2, cuff inner diameter: 2 mm, zero contact width. a–d: Fiber positions, see Fig. 5(a).

and 9 mm). In both cases the proximal anode, used to produce a complete block, has been spaced 3 mm from the cathode, being the minimum separation for blocking all fibers with low stimulus current (see above).

Fig. 7 shows the blocking thresholds at the distal anode for a 12 μm fiber (curve a1 and a2) at the axis of the nerve bundle and a 4 μm fiber (curve c1 and c2) at its border. Lowest thresholds were calculated for pulse durations just long enough to block the action potential at the node in plane with the anode. For shorter pulses the action potential has to be blocked at a node closer to the cathode. Due to a lower value of the activating function at this node, a higher current is necessary to block the action potential. Therefore, the curves of threshold versus pulse duration show a stepwise increase of blocking threshold with decreasing pulse duration.

If the distal anode is separated from the cathode by 6 mm, a pulse width of at least 220 μs is required to block the 12 μm fiber (curve a1) at minimum current while a pulse width of 390 μs is needed to block the 4 μm fiber (c1) as well. When taking into account the possibility of blocking at nodes closer to the cathode, there is a window of 190 μs (from 160 to 350 μs) in which all 12 μm fibers can be blocked without blocking any 4 μm fiber. The time window can be increased if the separation of cathode and distal anode is increased. At a contact separation of 9 mm, 270 μs is needed to block the 12 μm fiber (a2) at minimum current, while a 530 μs pulse is required to block the 4 μm fiber (c2). When taking into account blocking at other nodes, the window will be 270 μs (from 230 to 500 μs).

Apart from discriminating between large and small diameter fibers at the distal anode, the pulse duration should be adequate to block all fibers at the proximal anode at 3 mm from the cathode. This distance is the same in both configurations. The calculated values for a complete block at the proximal anode (4 μm fiber at the axis of the nerve bundle) are given by curve b in Fig. 7. It shows that a complete block requires a

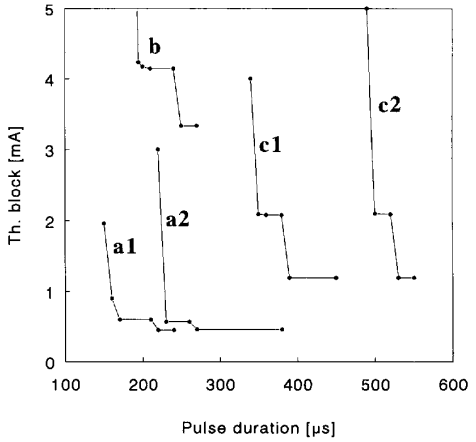

Fig. 7. Blocking thresholds (anodal current) as a function of pulse duration for two asymmetrical cuff electrodes. Contact separations: 3 mm (curve b) and 6 mm (curve a1 and c1) and 9 mm (curve a2 and c2). Cuff inner diameter: 2.4 mm. a1, a2: 12 μm fiber at axis of nerve bundle, b: 4 μm at axis of nerve bundle, c1, c2: 4 μm at border of nerve bundle.

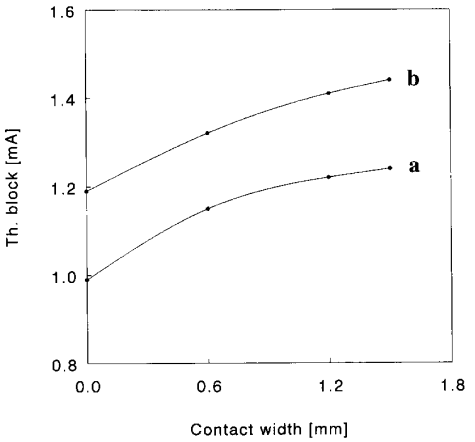

Fig. 8. Influence of contact width on the block thresholds (anodal current) of a 4 μm fiber at the border of the bundle. a: fiber with node under inner edge of electrode, b: fiber shifted over half the internodal distance.

pulse duration of at least 195 μs, reducing the window for a selective block from 190 μs to 155 μs in the configuration with an asymmetry ratio of 2. The window is not affected in case of an asymmetry ratio of 3, because a pulse duration of 230 μs required to block the 12 μm fibers exceeds the pulse duration required for a complete block. Therefore, a cuff electrode having a spacing ratio of 3 should be preferred.

D. Effect of Contact Width and Nodal Position on Blocking Threshold

The effects of contact width and nodal position on the blocking threshold will be most pronounced for a fiber close to the contacts. Therefore, a 4 μm fiber at the boundary of the bundle was considered. We observed that the main part of the current was injected into the medium at the edge of the anodal contact closest to the cathode. Thresholds are presented for two fiber positions exhibiting the largest difference in threshold: one having a node right under the edge of the anodal contact and another fiber shifted over half the internodal distance, which is 0.2 mm for a 4 μm fiber.

Fig. 8 shows the influence of contact width for the two positions. The fiber having a node in the plane of the contact edge has the lowest threshold (**a**). With increasing contact width both thresholds increase slightly. When the width is increased from 0.6 mm to 1.2 mm the thresholds only increased by 6%. The contact width had no influence on the absolute difference in blocking threshold between the two fiber positions.

IV. Discussion

The aim of this study was to determine the optimal geometric parameters for an asymmetric tripolar cuff electrode for the stimulation of sacral roots. Therefore, threshold currents for excitation and blocking of two nerve fibers with different diameters in the sacral root were calculated. We chose a 4 μm fiber and a 12 μm fiber diameter, representing fibers innervating the detrusor muscle and fibers innervating the external sphincter, respectively [27]. The proximal anode must block the action potentials of all fibers initiated at the cathode, while the distal anode should only block the induced activity in the 12 μm fibers, without blocking the 4 μm fibers. At the distal side the difference (selectivity) between the blocking thresholds of 4 μm and 12 μm fibers should be as large as possible. Apart from these functional goals, the dimensions of the cuff and the currents should be minimized.

To represent the biological volume conductor in a model with acceptable computational load, simplifying assumptions have been made with respect to the complexity and variability of the anatomy of the nerve roots. The nerve roots are considered to be cylindrical, while the nerve tissue is considered to be a homogeneous, anisotropic and frequency-independent volume conductor. Structures influencing the electrical conductivity of the nerve (such as blood vessels and connective tissue) were not considered.

The model used to simulate the electrical behavior of nerve fibers in a cuff electrode consists of two parts which are not coupled. As a consequence, any influence of currents generated by active fibers in the bundle on the electric field imposed on the fiber bundle by the applied currents has been neglected. These fiber currents will not influence excitation thresholds because most fibers will be inactive before excitation occurs. Therefore, only blocking thresholds will be affected. The extracellular potential gradients generated by active fibers will be larger when the nerve bundle is insulated than in a noninsulated situation [21]. In our configuration the bundle is only partially insulated by a cuff. The cuff ends are "short-circuited" by the CSF surrounding the cuff. The current generated by active fibers runs partly through the CSF and decreases the potential field. The blocking occurs at the anodes which are located at both cuff ends. At these ends we expect the extracellular potentials to be rather low because the anodes are very close to the "short-circuiting" bulk. Therefore the effect of generated active currents is expected to be very small and can thus be neglected.

In experiments on anodal blocking of peripheral nerves [12], [17], excitation of large fibers occurs near the anode

at the end of a long rectangular blocking pulse. This so-called anodal break excitation does not occur in the nerve fiber model. A gradual decrease of the current, as in quasitrapezoidal pulses, to eliminate the anodal break excitation in experiments, was therefore not necessary in our simulations. We compared blocking thresholds using a rectangular pulse and a quasitrapezoidal one in a few cuff configurations, but the differences appeared to be negligible. In order to validate the model, the rectangular pulses can be extended by a slow decay if necessary, to avoid anodal break excitation [17].

The propagation velocity in the model is 27 m/s and 67 m/s for the 4 μm and 12 μm fiber, respectively, if the nerve fibers are not affected by a depolarizing or hyperpolarizing electric field. These velocities were higher if the fiber was depolarized and lower if hyperpolarized. Moreover, the 4 μm fiber will have a larger delay before its excitation near the cathode than the 12 μm fiber. It is therefore difficult to relate the calculated pulse widths to the propagation velocities. Based on the velocities of the 12 μm and 4 μm fiber, it would take 45 and 111 μs, respectively, to proceed 3 mm (between 6 mm and 9 mm contact separation). This is roughly in agreement with the 50 and 140 μs delays from the simulations.

Only a few papers on sacral root stimulation give experimental data useful for a comparison with our modeling results. These studies deal with excitation of fibers by monopolar or bipolar stimulation and not with tripolar cuff electrodes. All papers report the possibility of activating the urethral sphincter without activating the detrusor, which is in agreement with our modeling results. However, most data on thresholds for sphincter and detrusor contraction are given in voltages rather than currents. The stimulation voltages are largely dependent on electrode impedances and will, therefore, vary among experiments. Tanagho *et al.* [36] reported stimulation currents between 3 mA and 8 mA, which would be just above the threshold at which detrusor responds. They used helical electrodes placed extradurally, where the roots are surrounded by an epineurium. A helix has a larger leakage current than a cuff. This may explain the high threshold currents in comparison to our theoretical data (less than 2 mA). Using book electrodes (contacts mounted in grooves cut into a block of insulating material [5]), Brindley *et al.* [7] measured 0.3 mA to 3.0 mA for the somatic threshold and 5 mA to 20 mA to achieve maximum detrusor response. No data is given on the electrode dimensions, although these are usually rather large. Their excitation threshold, however, fits a cuff diameter of 4.0 mm in Fig. 6(a) (after extrapolation of the curves).

Using standard "Brindley" electrode books (rectangular cross section, 2 × 3 mm) we recently measured an initial bladder response in three patients at about 0.7 mA and a maximum bladder pressure at about 2 mA. If we assume that initial detrusor response occurs when only small fibers at the boundary of the bundle are activated and maximum bladder pressure occurs when all small fibers in the root are activated, then these data fit our theoretical values for a cuff diameter of 2.6 mm and 2.8 mm respectively (Fig. 6(a)).

For a comparison of the modeling results on blocking with experimental results from literature, only a single paper could be found on blocking sacral roots [6]. In this paper results of blocking with electrode books in baboons were presented. Except for the contact separations, dimensions of the books are not given. For an electrode separation of 4.5 mm, blocking started at a total current of 4.6 mA. Since this current was applied to two anodes in parallel, the blocking threshold will have been 2.3 mA, being approximately 350% more than predicted by our model for a 12 μm fiber. This discrepancy may be due to the larger cross section of the book. They also found a minimum pulse duration for blocking over 200 μs. When contact separation was 6.0 mm we calculated a minimum pulse duration of 160 μs. This means that with 4.5 mm separation the minimum duration would even be shorter.

Van den Honert *et al.* [17] measured the effect of electrode spacing on blocking in peripheral nerve. They found an increase in threshold if the spacing decreased from 9 mm to 3 mm. Our model predicts almost no threshold variation when spacing exceeds 4.0 mm (Fig. 5(b) and (d)). This difference may be due to the presence of a perineurium around peripheral nerves. This small layer with low conductivity increases the electrical distance between contacts and nerve fibers. It can therefore be interpreted in this case as an increased inner diameter of the cuff electrode (Fig. 5(d)).

The model predicts that the smallest electrode separation to achieve a complete block at low stimulus current is 3 mm. To obtain a good selectivity between small and large fibers, the model predicts a large influence of pulse duration. The best selectivity occurs at a large electrode separation because in that case the time difference between the arrival at the anode of action potentials from large and small fibers will be large. According to the model a separation of 6–9 mm will be enough. This results in a maximum overall cuff length of 13 mm (contact width: 1 mm). In that case a pulse duration of 300 μs is sufficient. The current will depend on the ratio of the nerve root diameter and the cuff inner diameter. The contact width should be kept small (< 1 mm) because a large width increases thresholds.

Because the model predicts a relatively large amplitude range and a large pulse duration window for the selective blocking of large fibers without blocking the small ones, we expect that selective activation of the detrusor muscle is feasible. Based on this modeling study, cuff electrodes have been developed and are currently tested in acute animal experiments.

When applying this technique in patients, selective detrusor activation would result in more physiological bladder emptying at lower intravesical pressures as compared to other techniques. However, to avoid reflex incontinence, cutting the dorsal sacral roots to deafferent the bladder will still be necessary to abolish autonomic reflex contractions of the bladder.

APPENDIX

The electric potential field generated by the cuff electrode in a volume conductor can be described by Poisson's equation

$$\vec{\nabla}.(\bar{\bar{\sigma}}\vec{\nabla}\phi) = \vec{\nabla}.\vec{j}_s \tag{1}$$

where

$\bar{\bar{\sigma}}$ = conductivity tensor
ϕ = electric potential
$\vec{j}_s$ = source current density.

Considering the current source as point sources, each point source i can be described with an amplitude I_i multiplied with a delta function. Writing out the left-hand side of (1) in full and expressing the right-hand side as a summation of point sources gives

$$\frac{\partial}{\partial x}\left(\sigma_x \frac{\partial \phi}{\partial x}\right) + \frac{\partial}{\partial y}\left(\sigma_y \frac{\partial \phi}{\partial y}\right) + \frac{\partial}{\partial z}\left(\sigma_z \frac{\partial \phi}{\partial z}\right) = -\sum_i I_i \delta(x - x_i, y - y_i, z - z_i). \quad (2)$$

The volume conductor is rotation symmetric with the axis of the cuff electrode and nerve being equal to the symmetry axis of the model. Therefore the left-hand side of (2) can be expressed in cylindrical coordinates using the coordinate transformations of (3). When assuming (4), the result can be written as the left-hand side of (5). The right-hand side of (2) resembles N infinitely thin current rings with current I_n and radius R_n which can also be expressed in cylindrical coordinates (5).

$$r = \sqrt[2]{x^2 + y^2}$$
$$\theta = \arctan\left(\frac{y}{x}\right)$$
$$z = z \quad (3)$$
$$\sigma_x = \sigma_y \equiv \sigma_r. \quad (4)$$

The third term of the left-hand side of (5) equals zero because of rotational symmetry and vanishes. This gives the analytical expression (6) for the electrical potential ϕ.

$$\frac{\partial}{\partial r}\left(\sigma_r \frac{\partial \phi}{\partial r}\right) + \frac{1}{r}\sigma_r \frac{\partial \phi}{\partial r} + \frac{1}{r^2}\frac{\partial}{\partial \theta}\left(\sigma_r \frac{\partial \phi}{\partial \theta}\right) + \frac{\partial}{\partial z}\left(\sigma_z \frac{\partial \phi}{\partial z}\right) = -\sum_{n=1}^{N} \frac{I_n}{2\pi R_n}\delta(r - R_n, z - z_n) \quad (5)$$

$$\frac{\partial}{\partial r}\left(\sigma_r \frac{\partial \phi}{\partial r}\right) + \frac{\sigma_r}{r}\frac{\partial \phi}{\partial r} + \frac{\partial}{\partial z}\left(\sigma_z \frac{\partial \phi}{\partial z}\right) = -\sum_{N=1}^{N} \frac{I_n}{2\pi R_n}\delta(r - R_n, z - z_n) \quad (6)$$

where

ϕ	: electric potential
r	: radius
$\sigma_r = \sigma_r(r, z)$	: conductivity in r-direction
$\sigma_z = \sigma_z(r, z)$	: conductivity in z-direction
I_n	: current injected by ring n
R_n	: radius of ring n
$\delta(r - R_n, z - z_n)$	: delta function.

Because of inhomogeneities of the volume, no analytical solution of (6) can be found. To solve (6) numerically we used a finite difference technique in a grid with variable spacing. This involves discretization of (6) with spacing h and k defined as

in z-direction: $h_i = z_i - z_{i-1} \quad (i = 1..P-1)$
P is number of grid points in z-direction

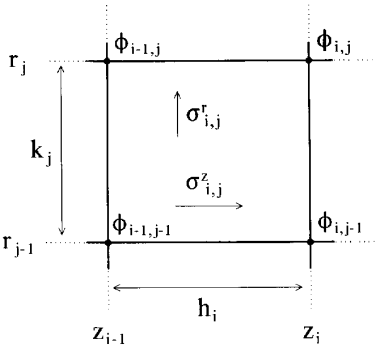

Fig. 9. Definitions of spacing and conductivities in grid.

in r-direction: $k_j = r_j - r_{j-1} \quad (j = 1..Q-1)$
Q is number of grid points in r-direction.

Equation (7) is the result of the first order discretization of (6).

$$\frac{\tilde{\sigma}^r_{i,j+1}\frac{\phi_{i,j+1}-\phi_{i,j}}{k_{j+1}} - \tilde{\sigma}^r_{i,j}\frac{\phi_{i,j}-\phi_{i,j-1}}{k_j}}{\frac{1}{2}(k_j + k_{j+1})} + \frac{1}{r}\bar{\sigma}^r_{i,j}(\phi_{i,j+1} - \phi_{i,j-1}) + \frac{\tilde{\sigma}^z_{i+1,j}\frac{\phi_{i+1,j}-\phi_{i,j}}{h_{i+1}} - \tilde{\sigma}^z_{i,j}\frac{\phi_{i,j}-\phi_{i-1,j}}{h_i}}{\frac{1}{2}(h_i + h_{i+1})} = \frac{-I_{i,j}}{\frac{1}{4}(h_i + h_{i+1})(k_j + k_{j+1})2\pi R_n} \quad (7)$$

where

$$\tilde{\sigma}^r_{i,j} = \frac{\sigma^r_{i,j} + \sigma^r_{i,j+1}}{2}$$
$$\tilde{\sigma}^z_{i,j} = \frac{\sigma^z_{i,j} + \sigma^z_{i+1,j}}{2}$$
$$\bar{\sigma}^r_{i,j} = \frac{\tilde{\sigma}^r_{i,j}\tilde{\sigma}^r_{i,j+1}}{k_j\tilde{\sigma}^r_{i,j+1} + k_{j+1}\tilde{\sigma}^r_{i,j}}(k_j + k_{j+1}). \quad (8)$$

The discrete conductivities $\sigma^r_{i,j}$ and $\sigma^z_{i,j}$ are defined as shown in Fig. 9. From (7) the potential $\phi_{i,j}$ can be isolated and expressed in the potentials of the neighboring grid points plus the current injected in point (i, j). The result is shown in (9) and (10).

As for boundary conditions, a Neumann condition ($\partial\phi/\partial r = 0$) was used at the symmetry axis ($r = 0$) while a Dirichlet condition ($\phi = 0$) was applied at the other three boundaries.

The set of linear equations (9) has been solved with the (iterative) successive relaxation method using a relaxation factor of 1.8.

The used dimensions were: 60×80 points, 40×18 mm, i.e., a cylinder with 40 mm length and 18 mm radius. The smallest spacing (0.3 mm in z-direction, 0.1 mm in r-direction) was used in the volume confined by the cuff.

A solution which meets our accuracy criterion (11) requires 5000 iterations (M: total grid points, k: iterations done).

$$\phi_{i,j} = \frac{\alpha\phi_{i-1,j} + \beta\phi_{i+1,j} + (\gamma - \epsilon)\phi_{i,j-1} + (\delta - \epsilon)\phi_{i,j+1} + I_d}{\alpha + \beta + \gamma + \delta} \quad (9)$$

$$\alpha = \frac{\tilde{\sigma}^z_{i,j}}{h_i(h_i + h_{i+1})} \quad \beta = \frac{\tilde{\sigma}^z_{i+1,j}}{h_{i+1}(h_i + h_{i+1})}$$
$$\gamma = \frac{\tilde{\sigma}^r_{i,j}}{k_j(k_j + k_{j+1})} \quad \delta = \frac{\tilde{\sigma}^r_{i,j+1}}{k_{j+1}(k_j + k_{j+1})} \tag{10}$$

$$\epsilon = \frac{\bar{\sigma}^r_{i,j}}{2r}$$

$$I_d = \frac{I_{i,j}}{(h_i + h_{i+1})(k_j + k_{j+1})\pi R_n}$$

$$\sum_{i=1}^{M} \left(\phi_i^{(k)} - \phi_i^{(k-100)}\right)^2 < 10^{-5}. \tag{11}$$

REFERENCES

[1] N. Accornero, G. Bini, G. L. Lenzi and M. Manfredi, "Selective activation of peripheral nerve fibre groups of different diameter by triangular shaped stimulus pulses," *J. Physiol.*, vol. 273, pp. 539–560, 1977.

[2] W. K. Altman and R. Plonsey, "A two-part model for determining the electromagnetic and physiologic behavior of cuff electrode nerve stimulators," *IEEE Trans. Biomed. Eng.*, vol. BME-33, pp. 285–293, 1986.

[3] W. H. Boyce, J. E. Lathem and L. D. Hundt, "Research related to the development of an artificial electrical stimulator for the paralyzed human bladder: A review," *J. Urol.*, vol. 91, pp. 41–51, 1964.

[4] I. A. Boyd and M. R. Davey, *Composition of peripheral nerves*. Edinburgh: Livingstone, 1968.

[5] G. S. Brindley, "An implant to empty the bladder or close the urethra," *J. Neurol. Neurosurg. Psych.*, vol. 40, pp. 358–369, 1977.

[6] G. S. Brindley and M. D. Craggs, "A technique for anodally blocking large nerve fibres through chronically implanted electrodes," *J. Neurol. Neurosurg. Psych.*, vol. 43, pp. 1083–1090, 1980.

[7] G. S. Brindley, C. E. Polkey and D. N. Rushton, "Sacral anterior root stimulators for bladder control in paraplegia," *Paraplegia*, vol. 20, pp. 365–381, 1982.

[8] G. S. Brindley, C. E. Polkey, D. N. Rushton and L. Cardozo, "Sacral anterior root stimulators for bladder control in paraplegia: The first 50 cases," *J. Neurol. Neurosurg. Psych.*, vol. 49, pp. 1104–1114, 1986.

[9] T. Brismar, "Potential clamp analysis of membrane currents in rat myelinated nerve fibres," *J. Physiol.*, vol. 298, pp. 171–184, 1980.

[10] S. Y. Chiu, J. M. Ritchie, R. B. Rogart and D. Stagg, "A quantitative description of membrane currents in rabbit myelinated nerve," *J. Physiol.*, vol. 292, pp. 149–166, 1979.

[11] R. E. Coggeshall, "Law of separation of function of spinal roots," *Physiol. Reviews*, vol. 60, pp. 716–755, 1980.

[12] Z.-P. Fang and J. T. Mortimer, "Selective activation of small motor axons by quasitrapezoidal current pulses," *IEEE Trans. Biomed. Eng.*, vol. 38, pp. 168–174, 1991.

[13] A. S. Ferguson, J. D. Sweeney, D. Durand and J. T. Mortimer, "Finite difference modelling of nerve cuff electric fields," *Proc. 9th Annu. Int. Conf. IEEE-EMBS*, pp. 1579–1580, 1987.

[14] L. A. Geddes and L. E. Baker, "The specific resistance of biological material—A compendium of data for the biomedical engineer and physiologist," *Med. & Biol. Eng.*, vol. 5, pp. 271–293, 1967.

[15] D. B. Halverstadt and W. L. Parry, "Electronic stimulation of the human bladder: 9 years later," *J. Urol.*, vol. 113, pp. 341–344, 1975.

[16] B. Holmquist and O. Tord, "Electromicturition in male dogs at pelvic nerve stimulation: an urethrocystographic study," *Scand. J. Urol. Nephol.*, vol. 2 (suppl. 2), pp. 115, 1968.

[17] C. van den Honert and J. T. Mortimer, "A technique for collision block of peripheral nerve: Single stimulus analysis," *IEEE Trans. Biomed. Eng.*, vol. BME-28, pp. 379–382, 1981.

[18] U. Jonas and E. A. Tanagho, "Studies on the feasibility of urinary bladder evacuation by direct spinal cord stimulation. II. Post stimulus voiding: a way to overcome outflow resistance," *Invest. Urol.*, vol. 13, pp. 151, 1975.

[19] P. E. V. van Kerrebroeck, E. Koldewijn, H. Wijkstra and F. M. J. Debruyne, "Intradural sacral rhizotomies and implantation of an anterior sacral root stimulator in the treatment of neurogenic bladder dysfunction after spinal cord injury; Surgical technique and complications," *World J. Urol.*, vol. 9, pp. 126–132, 1991.

[20] D. R. McNeal, "Analysis of a model for excitation of myelinated nerve," *IEEE Trans. Biomed. Eng.*, vol. BME-23, pp. 329–337, 1976.

[21] J. H. Meier, "Selectivity and design of neuro-electronic interfaces," Ph.D. Thesis, University of Twente, 1992.

[22] C. W. Morgan, W. C. de Groat, L. A. Felkins and S. J. Zhang, "Axon collaterals indicate broad intraspinal role for preganglionic neurons," *Proc. Natl. Acad. Sci. USA*, vol. 88, pp. 6888–6892, 1991.

[23] T. Morita, O. Nishizawa, H. Noto and S. Tsuchida, "Pelvic nerve innervation of the external sphincter of the urethra as suggested by urodynamic and horse-radish peroxidase studies," *J. Urol.*, vol. 131, pp. 591–595, 1984.

[24] F. Rattay, "Ways to approximate current-distance relations for electrically stimulated fibers," *J. Theor. Biol.*, vol. 125, pp. 339–349, 1987.

[25] F. Rattay, "Analysis of models for extracellular fiber stimulation," *IEEE Trans. Biomed. Eng.*, vol. 36, pp. 676–682, July 1989.

[26] G. Schalow, "The problem of cauda equina nerve root identification," *Zbl. Neurochirurgie*, vol. 46, pp. 322–330, 1985.

[27] G. Schalow, "Efferent and afferent fibres in human sacral ventral nerve roots: basic research and clinical implications," *Electromyogr. Clin. Neurophysiol.*, vol. 29, pp. 33–53, 1989.

[28] G. Schalow, "Oscillatory firing of single human sphincteric $\alpha 2$ en $\alpha 3$ motoneurons reflexly activated for the continence of urinary bladder and rectum. Restoration of bladder function in paraplegia," *Electromyogr. Clin. Neurophysiol.*, vol. 31, pp. 323–355, 1991.

[29] G. Schalow, "Number of fibres and fibre diameter distributions of nerves innervating the urinary bladder in humans. Acceptor nerve analysis. II (IV)," *Electromyogr. Clin. Neurophysiol.*, vol. 32, pp. 187–196, 1992.

[30] R. A. Schmidt, H. Bruschini and E. A. Tanagho, "Sacral root stimulation in controlled micturition. (Peripheral somatic neurotomy and stimulated voiding)," *Invest. Urol.*, vol. 17, pp. 130–134, 1979.

[31] J. J. Struijk, J. Holsheimer, G. G. van der Heide and H. B. K. Boom, "Recruitment of dorsal column fibers in spinal cord stimulation: Influence of collateral branching," *IEEE Trans. Biomed. Eng.*, vol. 39, pp. 903–912, 1992.

[32] J. D. Sweeney and J. T. Mortimer, "An asymmetric two electrode cuff for generation of unidirectionally propagated action potentials," *IEEE Trans. Biomed. Eng.*, vol. BME-33, pp. 541–549, 1986.

[33] J. D. Sweeney, J. T. Mortimer and D. R. Bodner, "Acute animal studies on electrically induced collision block for motor activity," *Neurourol. Urodyn.*, vol. 8, pp. 521–536, 1989.

[34] J. D. Sweeney, J. T. Mortimer and D. R. Bodner, "Animal study of pudendal nerve cuff implants for collision block of motor activity," *Neurourol. Urodyn.*, vol. 9, pp. 83–93, 1990.

[35] E. A. Tanagho and R. A. Schmidt, "Electrical stimulation in the clinical management of the neurogenic bladder," *J. Urol.*, vol. 140, pp. 1331–1339, 1988.

[36] E. A. Tanagho, R. A. Schmidt and B. R. Orvis, "Neural stimulation for the control of voiding dysfunction; A preliminary report in 22 patients with serious neuropathic voiding disorders," *J. Urol.*, vol. 142, pp. 340–345, 1989.

[37] J. W. Thüroff, M. A. Bazeed, R. A. Schmidt, D. M. Wiggin and E. A. Tanagho, "Functional pattern of sacral root stimulation in dogs: I. Micturition," *J. Urol.*, vol. 127, pp. 1031–1033, 1982.

[38] J. S. Walter, J. S. Wheeler, C. J. Robinson and R. D. Wurster, "Surface stimulation techniques for the bladder management in the spinal dog," *J. Urol.*, vol. 141, pp. 437–450, 1989.

[39] H. Wijkstra, N. J. M. Rijkhoff, J. Holsheimer, P. E. V. A. van Kerrebroeck, E. L. Koldewijn, H. B. K. Boom and F. M. J. Debruyne, "Selective stimulation and blocking of sacral nerves: research setup and preliminary results," *Proc. 13th. Annu. Int. Conf. IEEE-EMBS*, pp. 910–911, 1991.

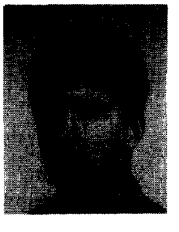

Nico J. M. Rijkhoff was born in Opneer, The Netherlands, in 1964. He received the M.Sc. degree in electrical and biomedical engineering in 1990 from the University of Twente, Enschede, The Netherlands. Since 1991, he has been working towards the Ph.D. degree at the Biomedical Engineering Group of the Department of Urology at the University Hospital Nijmegen, The Netherlands.

His research interests are related to electrical stimulation of the sacral nerve roots for restoration of urinary bladder control in spinal cord injury.

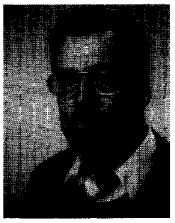

Jan Holsheimer was born in Enschede, The Netherlands, in 1941. He received the M.Sc. degree in Biology and Biophysics from the University of Groningen, The Netherlands, in 1965, and the Ph.D. degree in biomedical engineering from the University of Twente, Enschede, in 1982.

In 1965, he joined the Biomedical Engineering Division in the Department of Electrical Engineering at the University of Twente, where he was first engaged in the analysis and modeling of field potentials in the cortical brain structures. Since 1986, his primary research interests are theoretical, experimental and clinical studies of electrical nerve stimulation in spinal cord and peripheral nerves.

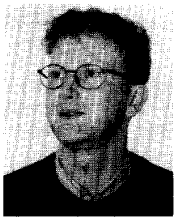

Evert L. Koldewijn was born in Hengelo, The Netherlands, in 1962. He received the M.D. degree from the Catholic University Nijmegen, in 1988. He is finishing his Ph.D. thesis on new developments in diagnosis and treatment of neurological disorders.

His research interests are in application of electrical neural stimulation for control of lower urinary tract dysfunctions and development of new diagnostic procedures for these disorders. He is currently resident in a general surgical department within the scope of his training as a urological surgeon.

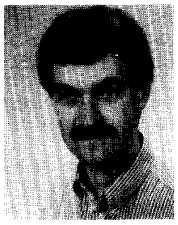

Johannes J. Struijk was born in Rijssen, The Netherlands, in 1963. He received the M.Sc. degree in electrical and biomedical engineering in 1988 and the Ph.D. degree in 1992 from the University of Twente, Enschede, The Netherlands. Since 1992, he has been working as a postdoctoral fellow in the Institute of Biomedical Technology at the University of Twente.

His research interests are related to spinal cord stimulation and nerve stimulation and include volume conduction and neural modeling.

Philip E. V. van Kerrebroeck was born in Louvain (Belgium) in 1953. He received the M.D. degree from the University of Louvain in 1978. Registered as a Urologist in 1984, he received the Masters degree in medicine from the University of Antwerp, Belgium, in 1992, and the Ph.D. degree in medical sciences from the University of Nijmegen, The Netherlands, in 1993.

He is working as a Urologist in the University Hospital of Nijmegen and is heading the Unit for Neurourology. His research is directed towards the development of new therapies in neurourology.

Frans M. J. Debruyne was born in Louvain, Belgium, in 1941. He received the M.D. degree from the University of Louvain in 1967 and the Ph.D. degree in medical sciences from the University of Nijmegen, The Netherlands, in 1977.

He was registered as a Urologist in 1973, and since 1979, he has been the head of the Department of Urology, University Hospital Nijmegen.

Hessel Wijkstra was born in Noordwijk, The Netherlands, in 1955. After polytechnics, he studied electrical engineering at the University of Twente, The Netherlands, and received the M.Sc. degree in 1984. He received the Ph.D. degree in 1989 from the Biomedical Engineering Division, University of Twente, for his research regarding deactivation in the rabbit heart.

He is currently a member of the staff of the Department of Urology, Radboud University Hospital Nijmegen, The Netherlands. He is the Head of the Biomedical Engineering Department. The main research topics of the Biomedical Engineering Department Unit are neurostimulation, digital image processing, medical artificial intelligence and urological system dynamics.